Comparison of Beam and Shell Theory for Mass Estimation in Preliminary Wing Design

Felix Dorbath, Björn Nagel, Volker Gollnick
German Aerospace Center (DLR), Air Transportation Systems

Abstract

This paper presents a comparison between the beam and shell theory for the application on wing box mass estimation in preliminary aircraft wing design. At first, the difference between the two theories in bending, in twist around the beam axis and in twist in flight direction is analyzed for a range of different wing geometries and load cases. In addition the differences in local and integral values of the x-normal, y-normal, xy-shear and von Mises stress are analyzed.
Afterwards, certain geometries are selected and a realistic aerodynamic load is applied. For those wings a sizing of the skin and spar thickness is performed using both, the beam and shell theory. The sizing is performed with constant aerodynamic loads as well as with aeroelastic loads.
Finally, explanatory statements for the differences in mass estimation and for different aeroelastic behaviour between both theories are discussed.

1. Introduction

In preliminary aircraft design a great number of unknown and versatile geometry parameters have to be determined. E.g. for the optimization of a wing, often thousands of loops with different geometry parameter modifications have to be performed. Therefore, fast methods are required to achieve results in an adequate computing time. To avoid modifications on basic design parameters in a later development phase, the chosen analysis methods have to be as accurate as possible.
The majority of today's tools for preliminary wing design are based on semi-physical models, using e.g. the beam theory for primary structural wing components combined with statistics for secondary masses. These models deliver accurate results for a typical aircraft, but have a decreasing level of confidence while deviating from typical design space. Due to the increased processing power of today's computers, simulation methods of a higher fidelity, e.g. the finite element shell theory, are applied more often.
Many studies have been performed using the beam theory (e.g. [1, 2, 3]) as well as the shell theory (e.g. [4, 5, 6]). But no widespread and systematic analysis of the differences between both theories with focus on mass estimation has been published so far.
On this account this study analyzes the differences between models based on finite shell theory and models based on the beam theory in preliminary wing design, focusing on their differences in mass estimation.
The study is performed in two steps: In the first step, the bending, the torsion and the stresses of more than 800 different wings with 6 different characteristic loads are analyzed. In the second step a few selected wings are computed, for which a sizing algorithm as well as a simple aerodynamic model are coupled to the structural models in order to identify the differences in mass estimation. Due to the high number of performed computations, an overview of the key results is presented in this paper.

2. Tools and Methods

Beam Model
As state-of-the-art, the beam model includes the front and rear spar, as well as the upper and lower skin between the two spars. Ribs as well as all other components (e.g. leading/trailing edges) are neglected.
For the beam model (compare [7]), the theory of bending according to Euler and Bernoulli [8, 9] and the theory of torsion according to St. Vénant [9, 10] for thin-walled closed section beams is used for the calculation of the displacements and stresses.
The Bernoulli assumptions for beams are as follows [9]:

- it is a slender beam (the length is much bigger than all other dimensions)
- the beam cross section, which was rectangular to the beam axis before bending, remains rectangular to the beam axis after bending
- the cross sections remains planar after bending

The Bernoulli beam represents two deformation modes: the first mode represents strain due to normal forces, the second represents bending due to bending moments. Deformation due to shear stresses is not covered by this beam model.
In any beam model, the planform is not exactly represented. At the beam model, all cross section are placed rectangular with respect to the beam axis. This is the axis in the geometric center of the

wing box, wherefore the planform at root and tip cannot be represented correctly (compare Fig. 1).

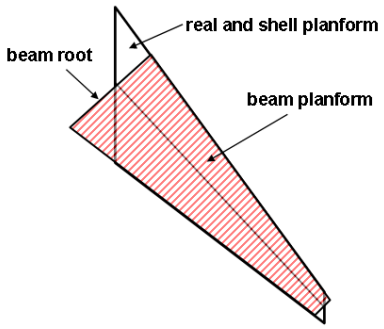

Fig. 1: Comparison of real, shell and beam wing planforms

Shell Model

The shell based wing model (compare [11]) includes the whole upper and lower skin, the front and rear spar as well as the ribs. The skins before respectively behind the wing box have a very small stiffness, so that the pressure load can be applied. Only neglectable stiffness is added to the overall wing stiffness due to these elements.

For the shell based wing model, finite element (FE) shell elements are used to model the skins, spars and ribs. For the linear analysis, the shell elements assumptions of thin plate behavior are:

- the thickness of the shell is much less than the next larger dimension
- the bending of the plate's midsurface is small compared with its thickness
- the midsurface remains unstrained (neutral) in case of bending due to loads that act normal to the plane midsurface
- the normal to the midsurface remains normal during bending.

Sizing Algorithm

Both models are sized with respect to the von Mises stress [12]. For the sizing process the models are split in 40 spanwise strips, in which the skin and spar thickness is constant. After computing the von Mises stress of all elements, the maximum von Mises stress of each spanwise strip is selected and used for the sizing of the whole strip.

The new skin and spar thickness is then computed by using the following formula:

$$t_{i+1} = t_i \cdot \frac{\sigma_{\max}}{\sigma_{allowed}} \qquad (1)$$

The skins and spars are sized independently. But the upper and lower skin as well as the front and rear spar are sized together. Otherwise the beam axis would not be longer located in the middle of the wing box, which is assumed for the whole computation.

Loads Cases and Aerodynamic Model

For the computation of the sizing with and without consideration of aeroelasticity the structural models are coupled with a simple aerodynamic model. The initial analysis of bending, torsion and stresses makes use of six exemplary characteristic load cases which are selected with the aim to cover those effects separately, which are important for the design of wings.

In detail the six chosen load cases are:

- tip loads in x-, y- and z-direction for the comparison of the basic effects (F_X, F_Y, F_Z)
- one rectangle and one triangle load, applied in the middle of the wing box (= beam axis) to apply a more realistic load distribution without torsion moments (F_{Zrect}, F_{Ztria})
- one rectangle load on the front spar, to include the additional effect of a torsion moment (F_{Zrect0})

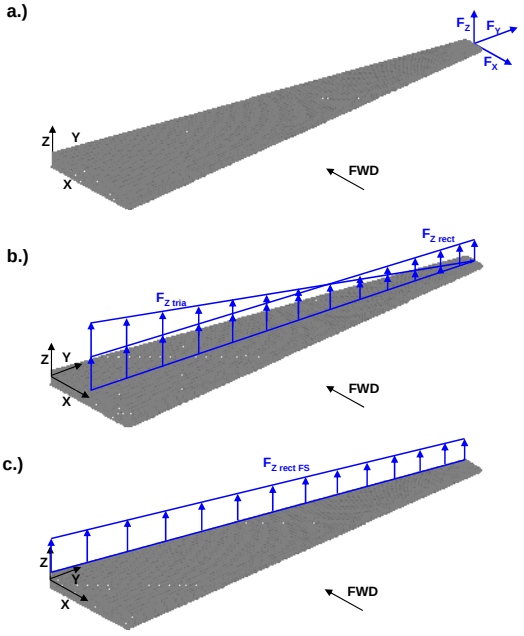

Fig. 2: a.) tip loads; b.) loads on beam axis; c.) load on front spar

For the aerodynamic computation, the program AVL (Athena Vortex Latice) of Prof. Mark Drela [13] is used for both structural models. AVL only computes a pressure-difference for each wing element. For the coupling of the aerodynamic and the shell model, the pressure-difference is split up into a pressure on the upper and the lower skin and interpolated on the structural grids by using the DLR inhouse interpolation routine gridapprox [14]. The split of the pressure is performed thusly, that 2/3 of the pressure force is acting on the upper skin, and 1/3 on the lower skin. Using this approach, the applied pressure distribution is not locally exact. But since this study focuses on the global influence of the aerodynamic loads on the wing and not on local effects, this method is well applicable.

Geometries

The geometries of the wings, analyzed in the first step, represent a variation of the basic wing design

parameters. Thereby values of realistic aircraft as well as more academic test cases are covered.
The geometries are split into 3 different groups. An overview of the geometries is given in Fig. 2 and Tab. 1.

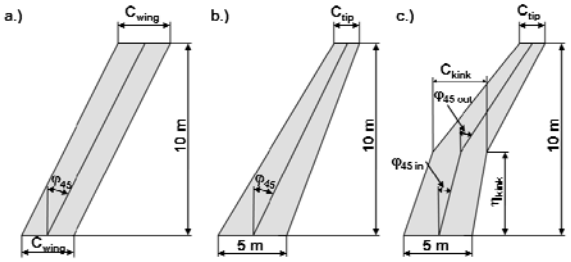

Fig. 3: Overview over wing box geometry groups A, B and C

Tab. 1: Details of wing geometry variation

group A: constant chord	
airfoil	symmetrical / rectangle
T/C	0.05 / 0.075 / 0.1 / 0.125 / 0.15 / 0.25 / 0.5
sweep [°]	0 / 10 / 20 / 30 / 40
chord [m]:	1 / 2 / 3 / 4 / 5
group B: constant root chord	
airfoil	symmetrical / rectangle
T/C	0.05 / 0.075 / 0.1 / 0.125 / 0.15 / 0.25 / 0.5
sweep [°]	0 / 10 / 20 / 30 / 40
tip chord [m]:	1 / 2 / 3 / 4 / 5
group C: kinked wings	
airfoil	symmetrical / rectangle
rel. kink position	0.3 / 0.6
T/C	0.15 / 0.25
sweep (in|out) [°]	0|0 / 0|20 / 0|40 / 20|40 / 40|0
chords (kink|tip) [m]	2.5|2 / 4.1|2 / 5|5

Each parameter in Tab. 1 is combined with the remaining values of the other parameters of each group. Together 820 different geometries are analyzed in the first step, under all 6 load cases.
For all wings the front spar is positioned at 20% of the wing chord and the rear spar is positioned at 70% of the chord. As the sweep refers to the middle of the beam axis in this study, it is the sweep at the 45%-line of the wing. The material of all wings is aluminium. The half span is constant for all wings and is 10 m, while the cords vary from 1 to 5 meter. Therefore aspect ratios between 4 and 20 are analyzed. For wing groups B and C the root chord is always 5 m.
All wings are clamped at the wing root, hence the centre wing box is not modelled.
For the analysis of the first step (bending, twist, and stresses) a constant skin and spar thickness of 5 mm is used.
For the second step, a much smaller amount of geometries is chosen. 5 different wings, equal to group A wings, are analyzed. The aspect ratio of those wings is 6.7, the thickness to chord ration (T/C) equals 12.5% and the sweeps range from 0° to 40°.

Comparisons
All relative differences, which are mentioned in the comparisons of this paper, are normalized with the shell results and are computed in the following way:

$$\Delta = \frac{value_{beam} - value_{shell}}{value_{shell}} \qquad (2)$$

3. Tip Displacement and Bending

The differences between the results of the beam and shell theory for unswept wings are mainly driven by additional bending caused by shear stresses. Fig. 3 depicts, that the bending angle of the shell model is constantly higher compared to the beam model. An analysis of the deformation of the shell elements shows, that the additional bending is caused by shear deformation of the elements. This additional bending is only computed in the shell theory as, according to the beam theory of Bernoulli, the shear stresses have no influence on bending. The relative size of the bending caused by shear stresses increases for small aspect ratios, high T/Cs as well as for small sweeps, compared with the bending due to bending moment. The application of the beam theory of Timoshenko instead of the beam theory according to Bernoulli would reduce this effect.

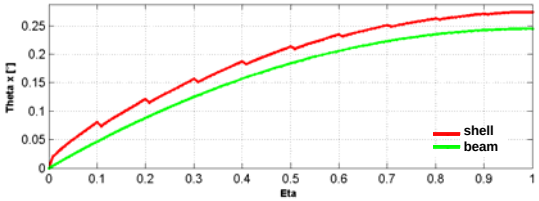

Fig. 4: Spanwise bending of the group A wing with rectangle airfoil, T/C = 0.5, sweep = 0°, chord = 5000 mm at F_Z tip load

Except the load case with a distributed triangle load in spanwise direction (F_{Ztria}), the differences in tip displacement of unswept wings are smaller than -1% for wings with an aspect ratio of 20, -3% for an aspect ratio of 10 and are up to -20% for an aspect ratio of 4 (compare Fig. 4).
For swept wings, minor differences occur due to two main reasons. On the one hand the influence of the bending caused by shear stresses decreases for growing sweeps due to an increasing aspect ratio of the beam. And on the other hand stiffens the skew clamping at the root, which is only taken into account in the shell theory computation, the structure in the root region. Therefore the additional bending, caused by shear stresses, is reduced.
The development of the differences for the F_{Ztria} load case is comparable with the other load cases. But the relative size of shear forces is higher compared with the size of the bending moment. Therefore the deformation caused by shear stresses is higher, wherefore the differences between the

two computation methods are still around -3% for unswept wings with an aspect ratio of 20.
The differences between the beam and shell theory at tapered wings (group B) are close to the differences of untapered wings (group A), having the same aspect ratio.

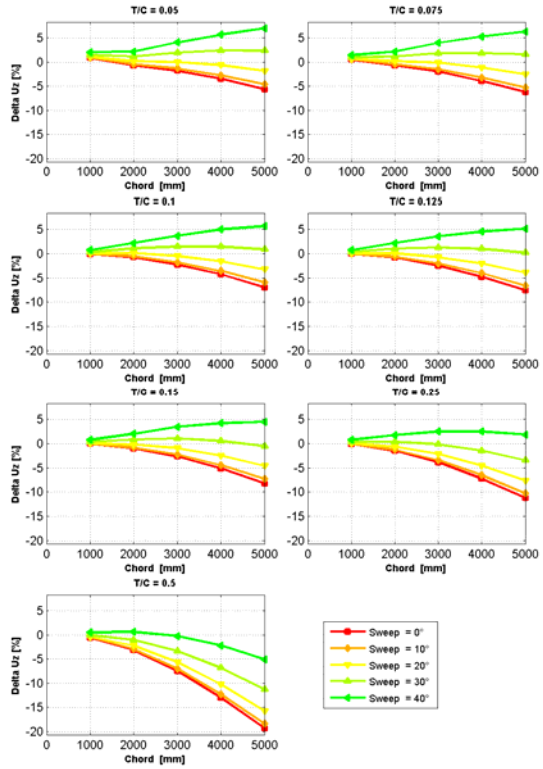

Fig. 5: Tip displacement of group A wings with rectangular airfoil under F_{Zrect} load

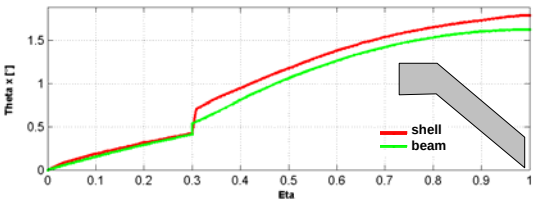

Fig. 6: Bending angle of group C wing with rectangular airfoil, T/C = 25%, sweeps = 40/0°, chord = 5m, F_Z

For wings, having geometry parameters comparable with current aircraft, the difference in the computation of the tip displacement between the two theories is smaller than ±5% for all load cases.
Kinks are not highly changing the spanwise bending behaviour of a wing. But directly at the kink position, steps in the spanwise bending angle distribution occur in both theories due to the different stiffness of the inner and outer wing. This step is often underestimated in the beam theory compared with the shell theory, wherefore kinked wings bend more in the shell computations.

4. Spanwise and Tip Torsion

There are three different reasons why an unkinked wing twists around the beam axis: torsion moment, skew clamping at the root as well as airfoils, for which the shear center not equals the beam axis.
The torsion caused by torsion moments is covered by both theories. For wings, having aspect ratios up to 10, the difference in torsion, computed via the two theories, is always smaller than ±5% (comp. Fig. 8; sweep = 0). At wings, having higher aspect ratios and small T/Cs, the difference is increasing up to -12%. The reasons for the differences between the two theories are on the one hand a lower torsion at the root of the wings computed via the shell theory. This is caused by the shear stress distribution at the root. On the other hand, an additional twist at the shell theory occurs due to shearing of the complete cross sections, while the cross section can not deform according to Bernoulli's beam theory.

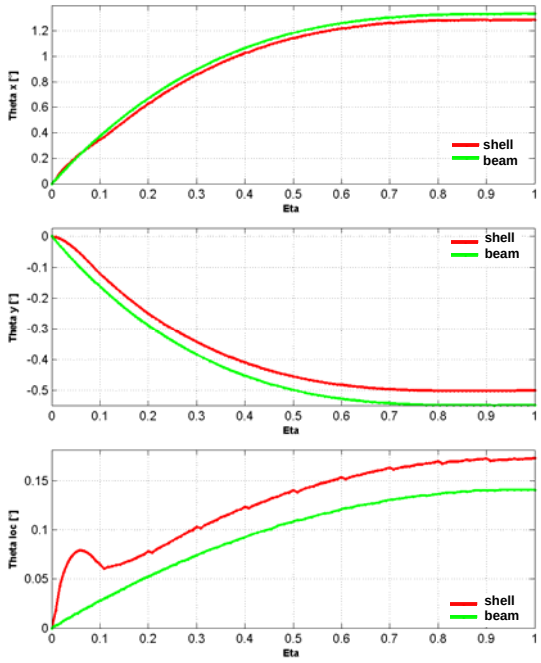

Fig. 7: Spanwise twist of 40° swept wing (T/C = 12.5%, chord = 3000mm, rectangle airfoil) under F_{Zrect0} load

The effect of the skew clamping on the torsion of the wing can be seen in Figs 7 and 8. In the lower graph of Fig. 7, the torsion around the beam axis in the beam computation is only caused by a torsion moment. In contrast, it can be clearly seen, that an additional twist appears close to the root in the shell computation caused by the skew clamping. Outbound of the first 20% of the span, both twist distributions are nearly parallel, which means, that the twist computations caused by torsion moment lay close together. The higher twist in the shell theory around the beam axis is reducing the forward twist around the global y-axis. That always appears at bending of swept wings (wash out effect), which can be seen in the middle graph of Fig. 7. Since the results for the bending lie close together, the difference can not be primary caused by the bending (upper graph in Fig. 7).
As it can be seen in Fig. 8, the sweep has a nameable influence on the difference in the

computation of the twist around the beam axis at the tip. At unswept wings, where only the torsion moment acts, the differences lie mostly beneath ±5%. For higher swept and untapered group A wings, the differences increases up to -20%. For tapered group B wings theses differences increase up to -30%.
The torsion, which is caused by different positions of the shear center and the beam axis at the cross sections, as it is the case at symmetrical airfoils, can only be covered by the shell theory. This effect causes a negative twist in the shell model, wherefore the difference for those group A wings with symmetrical airfoils are between +20% and +30% for unswept wings and between 0% and -10% for 40° swept wings.

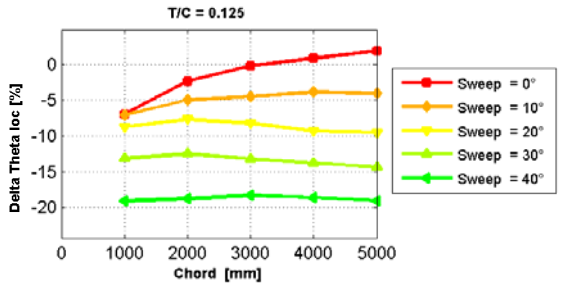

Fig. 8: Difference in twist around the beam axis at swept group A wings (rectangular airfoil, F_{Zrect0} load)

Transforming the twist around the beam axis to the twist around the global y-axis (=angle of attack) the twist is overlaid with the wash out effect. The wash out effect is directly related to the bending of the wing, wherefore the differences between the two theories in bending directly affect the wash out twist.
For wings having low sweeps, the highest differences between the beam and shell theories are caused by the symmetrical airfoil, because this effect always occurs, while the wash out effect as well as the skew clamping effect are small for small sweeps. The resulting differences in twist are up to -25% percent.
For higher sweeps, the wash out effect (and therefore the differences in bending) as well as the twist due to the skew clamping become more dominant. For wings with realistic geometry parameters the differences in twist around the global y-axis are between 0% and +10% for untapered wings and around +10% for tapered wings with rectangular airfoils. For wings having symmetrical airfoils and sweeps above 20°, the differences lay mostly around 10% below the differences of wings with rectangular airfoil.
The torsion, caused by torsion moments, only has little influence on the total difference in angle of attack computation. On the one hand, the differences there are relatively small and on the other hand, the torsion caused by torsion moments itself is small compared with the wash out effect.

5. Stress

The analysis of stresses is split into four parts: the analysis of x- and y- normal stresses, xy-shear stresses and the von Mises stress. As for aluminium wings the sizing of the skin and spar thicknesses is often based on the von Mises stress, the integral values of the von Mises stresses can be seen as a measurement for the wing weight.
The x-normal stresses, which are directed perpendicular to the beam axis, are always zero in the beam computations. At the computations with the shell theory, x-normal stresses occur close to the clamping at the root, directly at the ribs as well as close to the kink. Beside few outliers, the x-normal stresses are changing the integral von Mises stress in the shell computations between -1% and +3%.

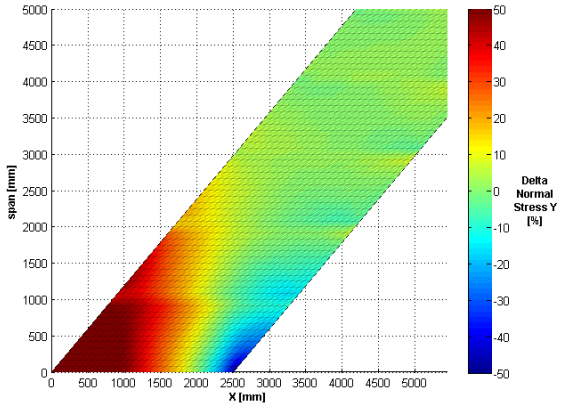

Fig 9: Difference of y_{BA}-normal stresses on the skin at the root of high swept wing

The differences in the computation of the integral y_{BA}-normal stresses, which are the stresses acting parallel to the beam axis, are small for unswept and untapered wings. For all of those calculations, the differences are smaller than ±2.5%.
At swept and untapered wings, the integral y-stress level computed via the beam theory is up to 9% higher for wings with 40° sweep and 5 m chord, than the stress level that is computed via shell theory. This is mainly caused by regions of higher and lower stresses close to the root at the shell computations, resulting in a lower integral stress level.
As the differences in the integral y-normal stresses are mainly induced by different stresses close to the root, the differences at tapered wings are similar to the differences of untapered wings having the same root chord.

The differences in shear stress computation differ compared with the other stress components. For unswept and untapered wings that have moderate or high aspect ratios and a rectangular airfoil, the shear stress level of the beam theory is up to 5% higher than the shear stress level according to the shell theory. There are three reasons for those

differences: the ribs are changing the shear stresses on the skin, the shear stresses in the shell theory are highly affected by the clamping at the root and are close to zero shortly before the tip. For small aspect ratios the differences can reach up to 10%.

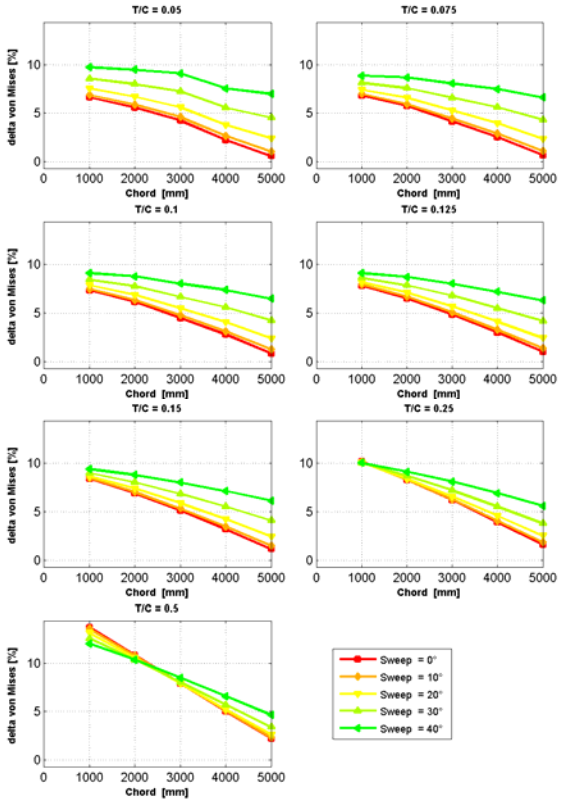

Fig. 10: Differences of von Mises stress for group B wings with rectangle airfoil and F_{Zrect} load case

For increasing sweeps, the relative shear stresses of the beam computation decrease and are between -10% and -20% lower for 40° swept wings. This is mainly caused by different shear stress distributions close to the skew clamping at the root, which is not taken into account in the beam computations.
The taper of the wings is significantly reducing the shear stresses in the shell computation, while the shear stresses in the beam computation are independent from the taper ratio. Therefore, the integral shear stress level of the beam theory is up to 2.5 times higher than the shear stresses in the shell computations for unswept wings.
There are methods to correct the shear stress distribution of the beam computation using analytical equations. But as these corrections are not part of the basic Euler-Bernoulli beam theory, they are not considered in this study.
These high differences between the two theories also lead to high differences in the computation of the main stress angle, which can reach up to 7° as an average over the whole skins and spars and much higher differences at some local positions.

The differences in the von Mises stresses are the result of the three stress components dominated by the y-normal stresses, which are clearly higher than the others. For untapered wings with realistic geometry parameters, the difference of the integral von Mises stress level is between +1% and +6%. At tapered wings with realistic geometry parameters, the relative von Mises stress level in the beam computation is higher, compared to the relative stress level at untapered wings, and can reach up to +9%. This is caused by the high differences of the shear stresses mentioned above.
The local differences in von Mises stresses are often higher than the integral values. Especially at the kink, the root as well as the area around the ribs, the values of the von Mises stress and the three stress components can differ strongly.

6. Sizing

The integral von Mises stress values, presented in the chapter before, are the integral values of each element. But for the sizing of the skins and spars, several elements are merged to areas of equal thicknesses, wherefore only the element having the highest stress level of each area impacts the sizing. Therefore, the wing weight is not only dependent on the integral value of the von Mises stress, also the stress distribution affects the wing weight.
In this chapter, an aerodynamic load is placed on a few group A wings (chord = 3m; T/C=12.5%; rectangular airfoil) and both structural models are coupled with a sizing algorithm.
In Fig. 11, the difference of the wing box mass for different sweeps is shown (red line). It can be seen, that the wing in the beam is always lighter than the shell wing, while the difference are smaller for low swept wings (-4%) and higher for higher sweeps (-17%). The differences of the integral stress values for these wings are between +2% and +4.5%. This means, that although the integral stress levels are higher for the unsized beam wings, the beam wings are lighter after sizing. Therefore, the maximum stress level per spanwise strip must be higher in the shell computation, although the integral value of all elements is lower.

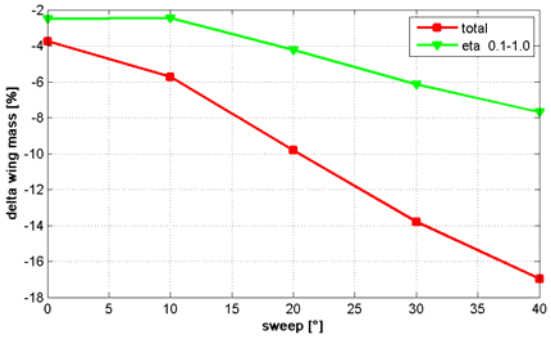

Fig. 11: Difference in wing box mass between beam and shell theory computations (group A; chord = 3m; T/C = 12.5%; rectangle airfoil, constant load)

The highest differences in local stresses can be found in the stress distribution at the rear part close

the root. As it can be seen in Fig. 9, high stress values occur in this region in the shell computation. Therefore, the shell thickness there is increased at the whole spanwise strip, although it would only be necessary at the rear part. This can nicely be seen in Fig. 12 where the skin thicknesses of a 40° swept wing is shown. Outside the innermost 20% of the span, the results between the two theories are close together (but the shell thickness is still higher), while the differences increase strongly within the first 20% of the span. Directly at the root, the skin thickness of the shell model is twice as high compared with the beam model.
How big the influence of the different thickness close to the root on the wing box mass is, can be seen at the green line in Fig. 11, which shows the difference of wing box mass, if only the outer 90% of the wing will be considered. It can be seen, that the differences are decreasing strongly, especially for higher swept wings. A third line, only considering the outer 80% percent, would show further decreased differences.

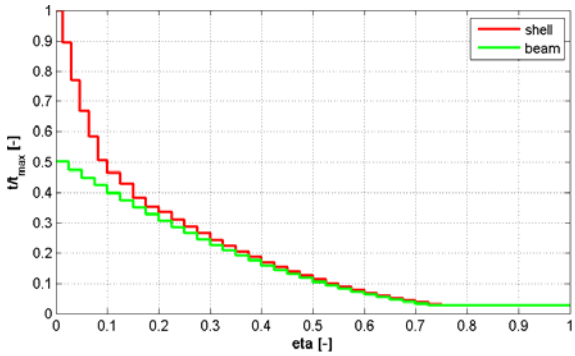

Fig. 12: Relative spanwise skin thickness distribution of 40° swept wing (group A; chord = 3m; T/C = 12.5%; rectangle airfoil)

As mentioned above, the skin thickness of the shell computations is also a bit thicker outside the root region and for unswept wings. This is caused, by a local higher stress level in the shell computation at the intersection between skins, spars and rips, which can not be covered by the beam theory.
For wings, having symmetrical airfoils this effect might be smaller. There the position of the elements, having the highest stress level, is more in the middle of the wing box and not close to the spars.

7. Aeroelasticity

Aerodynamic loads bend and twist wings simultaneously. Though total lift is kept constantly, the change in spanwise lift distribution affects a change in structural loads. To compute the correct wing mass, the loads have to be calculated considering aeroelastic interactions.
The aerodynamic load distribution is mainly depended on the spanwise angle of attack distribution, wherefore an accurate computation of the twist around the global y-axis is important. The highest influence on the twist around the global y axis is caused by the wash out effect, which appears due to bending on swept wings. In addition twist occurs due to torsion moments, skew clamping as well as airfoils having the shear center not in the middle of the wing box.

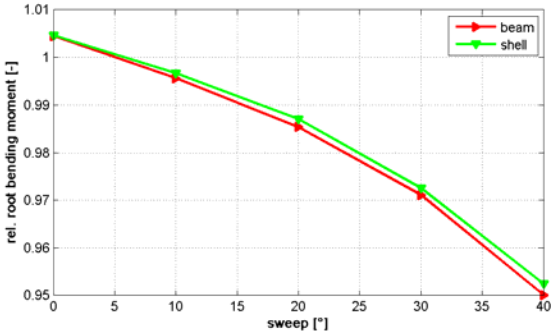

Fig. 13: Root bending moment of deflected and unsized wing compared with undeflected computation

In Fig. 13, the difference of the root bending moment between the undeformed and deflected wing for both theories is shown for unsized wings (= constant skin and spars thickness). It can clearly be seen, that the difference is small for wings having small sweeps and increases for higher swept wings. For 40° swept wings, the wing deformation leads to an around 5% lower root bending moment in the beam model. The root bending moment in the shell based wing model decreases less, compared with the beam model. This is caused by the negative twist due to the skew clamping in the shell model and reduces the aeroelastic effect around 5% compared with the beam model. But as the aeroelastic effect itself changes the root bending moment only around 5%, the absolute difference in bending moment is only 0.25% between the two theories.

8. Aeroelastic Sizing

In this chapter, the sizing is performed in the same way as in chapter 6, but the aerodynamic wing loading is continuously updated with respect to the wing deflection.
As it can be seen in Fig. 14, the differences in wing box mass are principally equal to the differences without updating the wing loads. While the differences in wing mass computation between the two theories are nearly identical for no and low swept wings, the differences are up to 2.4% higher for the 40° swept wing, which can be explained by two effects. On the one hand the shell beam bends less, wherefore the washout effect is smaller, which leads to a higher root bending moment (comp. Fig. 15). On the other hand, the positive twist, caused by the skew clamping, increases the angle of attack of the outer parts of the wing, and therefore is again reducing the washout effect. Therefore, the shell wing gets thicker skins and spars, which results in a

higher negative difference value in Fig. 14. The higher skin and spar thickness is increasing the stiffness of the model and therefore again reducing the wash out effect.

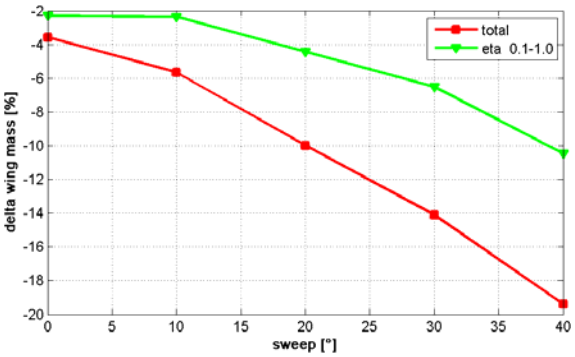

Fig. 14: Difference in wing box mass between beam and shell theory computations (group A; chord = 3m; T/C = 12.5%; rectangle airfoil, aeroelastic updated load)

The difference in the load computation that leads to a different wing weight is shown in Fig. 15. For unswept and low swept wings, the results of the root bending moment computation are very close together. For higher swept wings, the shell load is higher, compared with the shell load, due to the effect explained above.

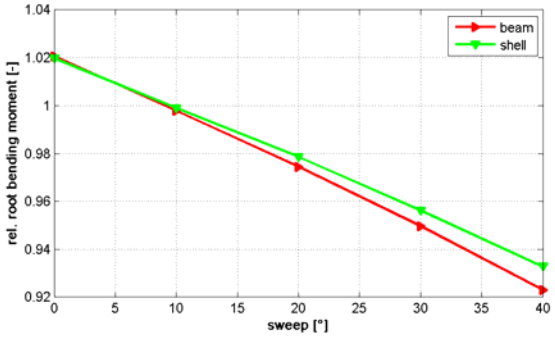

Fig. 15: Root bending moment of deflected and sized wing compared with undeflected computation

The differences between Figs 13 and 15 can be explained by the different deformation behavior of the sized and unsized wings. At the sized wings, the aeroelastic deformation of the wings is reducing the root bending moment up to 8%, compared with 5% at the unsized wing. Also the differences between the two theories are higher at the sized wings, because a higher load in the shell wing leads to higher skin and spar thicknesses, which increases the wing stiffness and therefore reduces the aeroelastic influence.
Although the differences in mass computation between the two theories do not change exceedingly, the absolute mass of the wings changes clearly. The effect of the aeroelastic computation is less then one percent for unswept wings in both theories. But for the 40° swept wing, the final wing box mass, computed using the beam theory gets up to 15% percent lighter, while the shell wing gets up to 13% lighter. This shows clearly, that the continuous update of the aerodynamic load is necessary for a good mass estimation for swept wings, while it is not absolutely necessary for un- or low swept wings of isotropic material.

9. Conclusion and Discussion

The analysis of the bending computation of the beam and the shell theory shows that the differences for wings, having realistic geometry parameters, are in general smaller than ±5%. The reasons for those differences are mainly caused by shear deformation, as well as the influence of the skew clamping in the shell model. In case of aeroelastic coupling, the bending mainly affects the wing load by the wash out effect, wherefore the wing bending is affecting the mass computation. For realistic wing geometry parameters, the differences in wing weight computation between the beam and shell theory is around 1% due to this effect at 40° swept wings.

The torsion caused by torsion moments is covered by both theories. The results are close enough together, that those differences are small compared to the total torsion.
The differences caused by torsion due to airfoils that do not have the shear center at the beam axis can have an influence on the torsion computation, dependent of the exact airfoil shape. But the wing boxes of airfoils that are currently in service often equal a rectangle, wherefore this effect should be small.
The torsion due to the skew clamping, which is only covered by the shell theory, has a high effect on the torsion around the beam axis, while the effect on the angle of attack change is much smaller as it is overlaid with the wash out effect. However, this effect still has a nameable impact on the global wing torsion and is reducing the aeroelastic influence and therefore the wing mass. The difference between the two theories caused by this effect result in around 1% different wing mass at 40° swept wings.

The integral stress level in the beam model of wings having realistic geometry parameters is up to 10% higher than the shell based wing model. The main reasons for the deviations are the differences in the shear stress computation, the stress distribution at the wing root as well as local differences at the intersections between ribs, spars and skins.
But although the integral stress level is higher in the beam computation, the beam wings are always lighter after sizing. This is because the sizing algorithm is computing the skin and spar thickness with respect to the maximum stress value at each spanwise strip. As also local effects are covered by the shell theory, the highest stress level per strip is

mostly higher in the shell computation than in the beam computation. Especially at the root clamping, high stress levels appear in the shell computation, which results in high differences in the sized material thicknesses and therefore in the absolute wing weight. This effect is the main driver for the large difference in wing weight computation of up to 19% for high swept wings.

As the high stress level only occurs at the rear part of the wing box, the skin and spar thickness at the forward part of the wing box is clearly bigger than is has to be in the shell computation. Therefore, the sizing strategy, which is chosen in this study, is not optimal. For swept wings, it would be better to split the regions of equal skin thicknesses in the shell computation spanwise and chordwise, to get a lighter wing. The beam theory can not cover this effect, wherefore it is impossible to compute the local skin thickness correctly. If only the global mass is of interest, the integrated beam results might be more accurate, than it seem to be according to the results of this study.
But also a chordwise split in 2 regions would still lead to a nameable higher wing weight in the shell computations. A further chordwise split in more regions of equal skin thicknesses would reduce the weight of the shell wing and therefore the differences in wing mass between the two structural theories. But here the question arises how many different chordwise splits make sense in terms of the production of an aircraft.

This study shows the main differences between the beam and shell theory with respect to wing mass estimation in preliminary aircraft design. All effects are shown on a range of example wing that have similar geometrical dimensions compared to real wings.
Referring to this study, the following tasks will be topic of follow-up analyses: the comparison and validation of the models on real wings as well as the analysis of the influence of anisotropic materials, where also the stress angles are relevant for sizing.

Acknowledgements

The Author would like to thank Samuel Polglase from the University of Adelaide for his support in developing and programming the beam model.

References

[1] Bindolino G., Ghiringhelli G., Ricci S., Terraneo M., Multilevel Structural Optimization for Preliminary Wing-Box Weight Estimation, Journal of Aircraft, Vol. 47, No. 2, 2010

[2] Van der Velden A., Kelm R., Kokan D., Mertens J., Application of MDO to Large Subsonic Transport Aircraft, 38th AIAA Aerospace Sciences Meeting & Exhibit, Reno, 2000

[3] Borglund D., Kuttenkeuler J., Active Wing Flutter Suppression using a Trailing Edge Flap, Journals of Fluids and Structures, Vol. 16, Issue 3, 2002

[4] Anhalt C., Monner H. P., Breitbach E., Interdisciplinary Wing Design – Structural Aspects, SAE International, 2003

[5] Kessler E., Laban M., Vankan W.J., Multidisciplinary Wing Optimisation, VIVACE Forum, 2005

[6] Jameson A., Vassberg J. C., Shankaran S., Aerodynamic-Structural Design Studies of Low-Sweep Transonic Wings, 46th AIAA Aerospace Sciences Meeting & Exhibit, 2008

[7] Wright J. R., Cooper E., Introduction to Aircraft Aeroelasticity and Loads, AIAA Education Series, 2007

[8] Timoshenko, S. P., History of strength of materials, New York, 1953

[9] Dieker S., Reimerdes H.G., Elementare Festigkeitslehre im Leichtbau, Donat Verlag, Bremen, 1992

[10] Connor J. J., Analysis of Structural Member Systems, Ronald Press Co., New York, 1976

[11] Premieniecki J.S., Finite Element Structural Analysis: new Concepts, AIAA Education Series, 2009

[12] von Mises R., Mechanik der festen Körper im plastisch-deformablen Zustand, Nachrichten von der Gesellschaft der Wissenschaften zu Göttingen, p 582-592, 1913

[13] Drela M., Youngren H., AVL V-3.26 user primer, MIT Department of Aero & Astronautical Engineering, April 2006

[14] Rose M., Nagel B., An Advanced Branch and Bound Method to interpolate acoustic data on Structural Finite Element meshes, ICSV13 conference, Vienna, 2006

Contact

Dipl.-Ing. Felix Dorbath
German Aerospace Center (DLR)
Air Transportation Systems
Blohmstraße 18
21079 Hamburg
Germany
Tel: 0049 (0)531-295-3829
e-mail: felix.dorbath@dlr.de